Inorg. Chem. **2002**, *41*, 5874–5881

Rotational Isomers of *N*-Alkylpyridylporphyrins and Their Metal Complexes. HPLC Separation, ^{1}H NMR and X-ray Structural Characterization, Electrochemistry, and Catalysis of $O_2^{\bullet-}$ Disproportionation

Ivan Spasojević,*,† Ramil Menzeleev,‡ Peter S. White,§ and Irwin Fridovich†

Department of Biochemistry, Duke University Medical Center, Durham, North Carolina 27710, Cirrus Pharmaceuticals, Inc., Research Triangle Park, North Carolina 27709-4748, and Department of Chemistry, University of North Carolina at Chapel Hill, Chapel Hill, North Carolina 27599

Received February 21, 2002

Rotational (atropo-) isomers of Mn(III) *meso*-tetrakis(*N*-alkylpyridinium-2-yl)porphyrins and corresponding metal-free porphyrin ligands (where alkyl is methyl, ethyl, *n*-butyl, *n*-hexyl) and Zn(II) *meso*-tetrakis(*N*-methyl(ethyl,*n*-hexyl)pyridinium-2-yl)porphyrins were separated and isolated by reverse-phase HPLC. The identity of the rotational isomers of metal-free *meso*-tetrakis(*N*-methylpyridinium-2-yl)porphyrin was established by ^{1}H NMR spectra and by the crystal structure of the fastest eluting fraction ($R_f = 7.7\%$, $R_w = 9.2\%$, $P2_1/c$, $Z = 8$, $a = 14.2846(15)$ Å, $b = 22.2158(24)$ Å, $c = 29.369(3)$ Å, $\beta = 95.374(2)°$) which, in accordance with ^{1}H NMR interpretation, proved to be the $\alpha\beta\alpha\beta$ isomer. This result, together with elution intensity patterns, was used to identify the fractions of other Mn(III)-porphyrins, Zn(II)-porphyrins, and corresponding metal-free ligands in the series. All of the atropoisomers were inert toward isomerization which was not observable for 30 days at room temperature and reached only 50% in 16 days at 90 °C in the case of the Mn(III)-ethyl analogue. However, a complete freeze-dry removal of the mobile phase from the HPLC fractions caused an almost 100% isomerization. The Mn(III) *meso*-tetrakis(*N*-ethylpyridinium-2-yl)porphyrin, as a mixture of atropoisomers (AEOL-10113), has been shown to offer protection in oxidative stress injury ascribed to its high reactivity toward superoxide ($k_{cat} = 5.8 \times 10^7$ M^{-1} s^{-1}) as a consequence of its favorable redox potential ($E_{1/2} = +228$ mV vs NHE). In this work, the atropoisomers were found to have similar redox potentials ranging from +240 to +220 mV, to be similarly potent catalysts of $O_2^{\bullet-}$ disproportionation (dismutation), with k_{cat} ranging from 5.5×10^7 to 6.8×10^7 M^{-1} s^{-1}, and not to preferentially bind to biological tissue.

Introduction

When *ortho* and *meta* substituted phenyls[1−4] and pyridyls[5] are placed at the *meso* positions of the porphyrin ring, they experience restricted rotation.[1−5] Consequently, such compounds exist as a mixture of 4 rotational isomers (atropoisomers), $\alpha\alpha\alpha\alpha$, $\alpha\alpha\alpha\beta$, $\alpha\alpha\beta\beta$, and $\alpha\beta\alpha\beta$, where "α" denotes an *N*-alkyl pointing above the porphyrin plane, and "*β*", below the plane (Scheme 1). On statistical grounds, the distribution of isomers in a mixture is expected to be $\alpha\alpha\alpha\alpha/\alpha\alpha\alpha\beta/\alpha\alpha\beta\beta/\alpha\beta\alpha\beta = 1{:}4{:}2{:}1$.[6,7] In practice, the ratio has been shown to deviate from this distribution and is affected by the size of the *ortho* substituent and by the type of the

* Corresponding author. E-mail: ivan@chem.duke.edu. Phone: (919) 684-2101.
† Duke University Medical Center.
‡ Cirrus Pharmaceuticals, Inc.
§ University of North Carolina at Chapel Hill.

(1) Bhatti, W.; Bhatti, M.; Eaton, S. S.; Eaton, G. R. *J. Pharm. Sci.* **1973**, *62*, 1574.
(2) Eaton, S. S.; Eaton, G. R.; Holm, R. H. *J. Organomet. Chem.* **1972**, *39*, 179.
(3) Eaton, S. S.; Eaton, G. R. *J. Am. Chem. Soc.* **1975**, *97*, 3660.
(4) Collman, J. P.; Brauman, J. I.; Doxsee, K.; Halbert, T. R.; Bunnenberg, E.; Linder, R. E.; LaMar, G. N.; Del Gaudio, J.; Lang, G.; Spartalian, K. *J. Am. Chem. Soc.* **1980**, *102*, 4182.
(5) (a) Mizutani, T.; Horiguchi, T.; Koyama, H.; Uratani, I.; Ogoshi, H. *Bull. Chem. Soc. Jpn.* **1998**, *71*, 413. (b) Iamamoto, Y.; Serra, O. A.; Idemori, Y. M. *J. Inorg. Biochem.* **1994**, *54*, 55−66.
(6) Gottwald, L. K.; Ullman, E. F. *Tetrahedron Lett.* **1969**, 3071.
(7) Walker, F. A. *Tetrahedron Lett.* **1971**, 4949.

10.1021/ic025556x CCC: $22.00
Published on Web 10/08/2002

Scheme 1. Most Abundant Rotational (Atropo-) Isomer ($\alpha\alpha\alpha\beta$) of Mn(III) *meso*-Tetrakis(*N*-alkylpyridinium-2-yl)porphyrins, $Mn^{III}T(alkyl)$-2-PyP^{5+} [a]

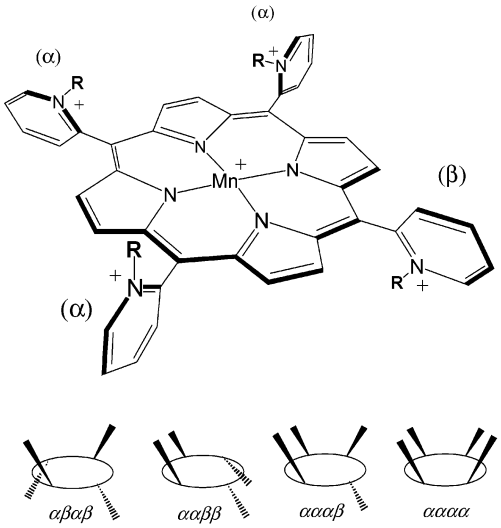

[a] Alkyl (i.e., R in this scheme) groups consist of methyl, ethyl, *n*-butyl, and *n*-hexyl. Other atropoisomers are represented only schematically.

metal coordinated.[8] By employing different techniques, a partial enrichment of the mixture in a particular atropoisomer was also reported.[9,10] When *ortho*-substituted phenyls are bulky, such as sterically encumbered naphthyl,[11] *N*-methylnicotinamidophenyl,[12,13] and *N*-methylisonicotinamidophenyl[14] groups, the separation and the isolation of the atropoisomers of such porphyrins is rather straightforward. However, the separation and isolation of atropoisomers of a porphyrin which is *meso*-substitituted by less bulky *N*-methylpyridyl groups is less efficient.[15] The atropoisomers of Zn(II), Ni(II), and Cu(II) *meso*-tetrakis(*N*-methylpyridyl)-porphyrin were successfully separated and isolated by normal-phase chromatography by Kaufmann et al.[15] However, the atropoisomers of the metal-free ligand (H_2TM-2-PyP^{4+}) and its Mn(III) complex (Mn^{III}TM-2-PyP^{5+}) have not been isolated.[15] [The following abbreviations will be used throughout the text: $Mn^{III}T(alkyl)$-2-PyP^{5+}, manganese(III) 5,10,15,20-tetrakis(*N*-alkylpyridinium-2-yl)porphyrin; alkyl is M, methyl; E, ethyl; Bu, *n*-butyl; Hex, *n*-hexyl; 2 identifies the ortho isomer; $H_2T(alkyl)$-2-PyP^{4+}, 5,10,15,20-tetrakis-(*N*-alkylpyridinium-2-yl)porphyrin; H_2T-2-PyP^{4+}, 5,10,15,-20-tetrakis(pyridinium-2-yl)porphyrin; ZnTM(E,Hex)-2-PyP^{4+}, zinc(II) 5,10,15,20-tetrakis(*N*-methyl(ethyl,*n*-hexyl)-pyridinium-2-yl)porphyrin.]

We have shown previously that the Mn^{III}TM-2-PyP^{5+} (AEOL-10112) and its ethyl analogue, Mn^{III}TE-2-PyP^{5+} (AEOL-10113), (both as mixtures of atropoisomers) are potent porphyrin-based catalysts of $O_2^{\bullet-}$ disproportionation (dismutation) with a log k_{cat} value of 7.8.[16−18] The log k_{cat} for the Cu,Zn-SOD (SOD = superoxide dismutase) is ∼9.3.[19−21] Thus, the catalytic potency of the Mn^{III}TM(E)-2-PyP^{5+} is ∼3% of the potency of the enzyme itself, on a molar basis.

Moreover, they offered protection in different models of oxidative stress diseases such as diabetes,[22] stroke,[23] sickle-cell disease,[24] liver ischemia,[25] and radiation/cancer.[26,27] Because these Mn(III) porphyrins are potential drug candidates, characterization of their atropoisomers is important. In a preliminary HPLC study, utilizing electrochemical detection, the atropoisomers of Mn^{III}TE-2-PyP^{5+} were separated.[28] As they were not structurally characterized, the assumed identity provided by authors proved to be incorrect as shown in this work.[28]

In this work, we report an improved separation and isolation of the atropoisomers of Mn(III) *meso*-tetrakis(*N*-alkylpyridinium-2-yl)porphyrins (including Mn^{III}TE-2-PyP^{5+}) and the corresponding metal-free porphyrin ligands (where *alkyl* is methyl, ethyl, *n*-butyl, and *n*-hexyl) and Zn(II) *meso*-tetrakis(*N*-methyl,ethyl,*n*-hexylpyridinium-2-yl)porphyrin by UV−vis HPLC as well as the identification of separate fractions supported by ^{1}H NMR and X-ray crystallography. A number of X-ray structures of *meso*-tetrakis(phenyl)-porphyrins[29−34] and the atropoisomers of their *ortho*-

(8) Freitag, R. A.; Whitten, D. G. *J. Phys. Chem.* **1983**, *87*, 3918
(9) Lindsey, J. *J. Org. Chem.* **1980**, *45*, 5215.
(10) Elliot, C. M. *Anal. Chem.* **1980**, *52*, 666.
(11) Thrash, T. P.; Wilson, L. J. *Inorg. Chem.* **2001**, *40*, 4556.
(12) Buckingham, D. A.; Gunter, M. J.; Mander, L. N. *J. Am. Chem. Soc.* **1978**, *100*, 2899.
(13) Miskelly, G. M.; Webley, W. S.; Clark, C. R.; Buckingham, D. A. *Inorg. Chem.* **1988**, *27*, 3773.
(14) Valiotti, A.; Adeyemo, A.; Williams, R. F. X.; Ricks, L.; North, J.; Hambright, P. *J. Inorg. Nucl. Chem.* **1981**, *43*, 2653.
(15) Kaufmann, T.; Shamsai, B.; Song Lu, R.; Bau, R.; Miskelly, G. M. *Inorg. Chem.* **1995**, *34*, 5073.
(16) Batinić-Haberle, I. *Methods Enzymol.* **2002**, *349*, 223.
(17) Spasojević, I.; Batinić-Haberle, I. *Inorg. Chim. Acta* **2001**, *317*, 230.
(18) Batinić-Haberle, I.; Spasojević, I.; Hambright, P.; Benov, L.; Crumbliss, A. L.; Fridovich, I. *Inorg. Chem.* **1999**, *38*, 4011.
(19) Vance, C. K.; Miller, A.-F. *J. Am. Chem. Soc.* **1998**, *120*, 461.
(20) Ellerby, R. M.; Cabelli, D. E.; Graden, J. A.; Valentine, J. S. *J. Am. Chem. Soc.* **1996**, *118*, 6556.
(21) Klug-Roth, D.; Fridovich, I.; Rabani, J. *J. Am. Chem. Soc.* **1973**, *95*, 2786.
(22) Piganelli, J. D.; Flores, S. C.; Cruz, C.; Koepp, J.; Batinić-Haberle, I.; Crapo, J. D.; Day, B. J.; Kachadourian, R.; Young, R.; Bradley, B.; Haskins, K. *Diabetes* **2002**, *51*, 347.
(23) Mackensen, G. B.; Patel, M.; Sheng, H.; Calvi, C. L.; Batinić-Haberle, I.; Day, B. J.; Liang, L. P.; Fridovich, I.; Crapo, J. D.; Pearlstein, R. D.; Warner, D. S. *J. Neurosci.* **2001**, *21*, 4582.
(24) Aslan, M.; Ryan, T. M.; Adler, B.; Townes, T. M.; Parks, D. A.; Thompson, J. A.; Tousson, A.; Gladwin, M. T.; Patel, R. P.; Tarpey, M. M.; Batinić-Haberle, I.; White, C. R.; Freeman, B. A. *Proc. Natl. Acad. Sci. U.S.A.* **2001**, *98*, 15215.
(25) Parks, D.; Fridovich, I.; O'Donnell, V. B.; Wang, Z.; Batinić-Haberle, I.; Day, B. J.; Chumley, P. H.; Freeman, B. A. *Free Radic. Biol. Med.* **1998**, *25* (Suppl. 1), S36.
(26) (a) Batinić-Haberle, I.; Spasojević, I.; Fridovich, I.; Anscher M. S.; Vujašković, Z. *Int. J. Radiat. Oncol. Biol. Phys.* **2001**, *51* (Suppl. 1), 235. (b) Vujašković, Z.; Batinić-Haberle, I.; Spasojević, I.; Samulski, T. V.; Fridovich, I.; Dewhurst, M. W.; Anscher, M. S. *Proc. of the 48th Annual Meeting of the Radiation Research Society*, San Juan, Puerto Rico, 2001, p 160. (c) Vujašković, Z.; Batinić-Haberle, I.; Spasojević, I.; Fridovich, I.; Dewhurst, M. W.; Anscher, M. S. *Free Radic. Biol. Med.* **2001**, *31* (Suppl. 1), S128.
(27) Vujašković, Z.; Batinić-Haberle, I.; Rabbani, Z. N.; Feng, Q.-F.; Kang, S. K.; Spasojević, I.; Samulski, T. V.; Fridovich, I.; Dewhirst, M. W.; Anscher, M. S. *Free Radic. Biol. Med.* **2002**, *33*, 857.
(28) Kachadourian, R.; Menzeleev, R.; Bushra, A.; Bocckino, S. B.; Day, B. J. *J. Chromatogr., B* **2002**, *767*, 61.
(29) Senge, M. O. Database of Tetrapyrrole Crystal Structure Determinations. In *The Porphyrin Handbook*; Academic Press: San Diego, CA, 2000.
(30) Tulinsky, A.; Chen, B. M. L. *J. Am. Chem. Soc.* **1977**, *99*, 3647.
(31) Hoard, J. L.; Cohen, G. H.; Glick, M. D. *J. Am. Chem. Soc.* **1967**, *89*, 1992.
(32) Fleischer, E. B.; Miller, C. K.; Webb, L. E. *J. Am. Chem. Soc.* **1964**, *86*, 2342.

substituted analogues[35−38] have been reported, yet only a few *para meso*-tetrakis(pyridyl)porphyrins[39,40] and their *N*-alkylated analogues[41−44] have been structurally characterized. Further, only a metal complex with the atropoisomer of *ortho meso*-tetrakis(*N*-methylpyridyl)porphyrin, specifically $\alpha\alpha\alpha\beta$ Cu^{II}TM-2-PyP^{4+}, was previously characterized by X-ray crystallography.[15] The X-ray structure of the $\alpha\beta\alpha\beta$ H_2TM-2-PyP^{4+} solved in this work is the first report on the atropoisomer of an *ortho meso*-tetrakis(*N*-alkylpyridyl)porphyrin ligand. Preparation of crystals of the Mn(III) and Zn-(II) complexes with atropoisomers of H_2TM-2-PyP^{4+} is in progress.

An evaluation of the chemical and biological activity of atropoisomers of Mn^{III}TE-2-PyP^{5+} includes measurements of $E_{1/2}$ and k_{cat} for $O_2^{\bullet-}$ disproportionation, and those data are reported herein.

Experimental Section

Materials. General. $MnCl_2 \cdot 4\,H_2O$, *iso*-amyl alcohol and Baker-flex silica gel IB were purchased from J. T. Baker. *N*,*N*′-Dimethylformamide, ethyl *p*-toluenesulfonate, 2-propanol (99.5+ %), NH_4PF_6 (99.99%), NaCl, and tetrabutylammonium chloride were from Sigma-Aldrich, while xanthine and ferricytochrome *c* were purchased from Sigma. *n*-Butyl *p*-toluenesulfonate and *n*-hexyl *p*-toluenesulfonate were from TCI America. Methanol (anhydrous, absolute), ethanol (absolute), acetone, ethyl ether (anhydrous), chloroform, and KNO_3 were from Mallinckrodt. Acetonitrile and trifluoroacetic acid were from Fisher Scientific, and triethylamine was from Pierce. Xanthine oxidase was prepared by R. Wiley and was supplied by K. V. Rajagopalan.[45] Catalase was from Boehringer, ultrapure argon was from National Welders Supply Co, and phosphate-buffered saline was from Life Technologies.

Porphyrins. The non-*N*-alkylated precursor ligand, H_2T-2-PyP, and its *N*-methylated analogue, H_2TM-2-PyP^{4+}, were obtained from Mid-Century Chemicals, Chicago, IL, and used without further purification. The preparation of other *N*-alkylpyridylporphyrins (alkyl being ethyl, *n*-butyl, and *n*-hexyl), the insertion of manganese, and the characterization of the ligands and their Mn(III) complexes were performed as previously reported.[16−18] ZnTM-2-PyP^{4+} and ZnTE-2-PyP^{4+} were previously characterized.[46] The insertion of zinc into H_2THex-2-PyP^{4+} was done as described for the metalation of H_2TM(E)-2-PyP^{4+}.[46] The UV−vis spectral data for ZnTHex-2-PyP^{4+} follow. λ_{max}(log ϵ): 264.0 nm (4.43), 328.0 nm (4.49), 427.0 nm (5.64), 557.5 nm (4.40), 594.0 nm (3.88). Anal. Calcd for ZnTHex-2-$PyP^{4+}\cdot 11.5H_2O$ ($ZnC_{64}H_{99}N_8O_{11.5}Cl_4$): C, 56.04; H, 7.27; N, 8.17. Found: C, 55.96; H, 6.42; N, 8.60. The characterization of higher analogues of *N*-alkylpyridylporphyrins[47,48] and their Mn(III) complexes is reported elsewhere.[47]

Methods. HPLC Separation. Reversed-phase liquid chromatography of Mn^{III}TE-2-PyP^{5+} was performed on a YMC-Pack, ODS-AM column (3 μm particle size, 120 Å pore size, 150 mm long × 4.6 mm i. d.) mounted on an Agilent Technologies (former Hewlett-Packard) 1100 series HPLC system (vacuum degasser, quaternary pump, UV−vis diode-array detector with 13 μL, 10 mm path-length cell, and HP Chem-Station software). All experiments were performed with the column immersed in a water bath at 45 ± 0.2 °C. Solvent A: deionized water, 20 mM triethylamine, pH 2.7 adjusted with concentrated trifluoroacetic acid. Solvent B: acetonitrile, HPLC grade. The flow rate in all experiments was 1 mL/min, and the "dead volume" of the column together with tubing was ∼2 mL. Thus, the "dead time" of acquisition was approximately 2 min. Typical back-pressure was 120−130 bar depending on the amount of acetonitrile in the mobile phase. All samples were diluted in at least 90% of solvent A prior to injection of 5−10 μL into a 20 μL sample loop. Quantitative preparations were conducted on the same column by pooling fractions collected after several consecutive 10 μL injections of 10 mM porphyrin dissolved in solvent A. The final volume of each pooled fraction was ∼2 mL containing 0.1−0.4 mM porphyrin. For all of the compounds studied, the same conditions were applied except for the acetonitrile content in the mobile phase. The conditions employed for a complete separation of atropoisomers are given in Table 1. Throughout the text, the fractions are enumerated from 1 to 4, with 1 being the fraction coming first out of the column (shortest retention time).

^{1}H NMR. Solvent was removed from 0.5 mL of each pooled HPLC fraction (see previous description) almost to dryness under mild vacuum at room temperature. Then, 0.7 mL of D_2O (99.9%, Cambridge Isotope Laboratories) was added and stirred, and the sample was transferred into a grade 6 KONTES NMR tube (∼100 μM porphyrin). All ^{1}H NMR measurements were done on a Varian 500 MHz instrument. The 128 spectra were collected in H_2O-suppression mode, averaged, and phase-corrected in "manual" mode.

X-ray Structure. Into 1.5 mL of each pooled fraction of H_2-TM-2-PyP^{4+} prepared for NMR analysis, $NaClO_4$ was added to a final concentration of 20 mM. After 2 days under mild vacuum at room temperature, needlelike crystals appeared. Only the crystals of the *first* fraction were suitable for X-ray crystallography analysis. The X-ray crystal structure was solved at the University of North Carolina at Chapel Hill. A dark red-brown crystal (0.3 × 0.2 × 0.005 mm^3 needlelike plate) was mounted on a Bruker SMART diffractometer, and 16078 unique (5463 significant) reflections were collected at −100 °C in "ω scan" mode. A summary of cell constants and refinement data is given in Table 2. ORTEP diagrams (Figures S1 and S2), selected out-of-plane distances (Tables S1 and S2), and plane-to-plane angles (Table S3) are given in the

(33) (a) Silvers, S.; Tulinsky, A. *J. Am. Chem. Soc.* **1964**, *86*, 927. (b) Silvers, S.; Tulinsky, A. *J. Am. Chem. Soc.* **1967**, *89*, 3331.
(34) La, T.; Miskelly, G. M.; Bau, R. *Inorg. Chem.* **1997**, *36*, 5321.
(35) Miskelly, G. M.; Webley, W. S.; Clark, C. R.; Buckingham, D. A. *Inorg. Chem.* **1988**, *27*, 3773.
(36) Nasri, H.; Ellison, M. K.; Chen, S.; Huynh, B. H.; Scheidt, W. R. *J. Am. Chem. Soc.* **1997**, *119*, 6274.
(37) Jagessar, R. C.; Shang, M.; Scheidt, W. R.; Burns, D. H. *J. Am. Chem. Soc.* **1998**, *120*, 11684.
(38) Collins, D. M.; Hoard, J. L. *J. Am. Chem. Soc.* **1970**, *92*, 3761.
(39) Endisch, C.; Fuhrhop, J.-H.; Buschmann, J.; Luger, P.; Siggel, U. *J. Am. Chem. Soc.* **1996**, *118*, 6671.
(40) Collins, D. M.; Hoard, J. L. *J. Am. Chem. Soc.* **1970**, *92*, 3761.
(41) (a) Ivanca, M. A.; Lappin, A. G.; Scheidt, W. R. *Inorg. Chem.* **1991**, *30*, 711. (b) Kirner, J. F.; Garofalo, J., Jr.; Scheidt, W. R. *Inorg. Nucl. Chem. Lett.* **1975**, *11*, 107.
(42) Körber, F. C. F.; Lindsay Smith, J. R.; Prince, S.; Rizkallah, P.; Reynolds, C. D.; Shawcross, D. R. *J. Chem. Soc., Dalton Trans.* **1991**, 3291.
(43) Prince, S.; Körber, F.; Cooke, P. R.; Lindsay Smith, J. R.; Mazid, M. A. *Acta Crystallogr.* **1993**, *C49*, 1158.
(44) Ford, K. G.; Pearl, L. H.; Neidle, S. *Nucleic Acids Res.* **1987**, *15*, 6553.
(45) Waud, W. R.; Brady, F. O.; Wiley, R. D.; Rajagopalan, K. V. *Arch. Biochem. Biophys.* **1975**, *19*, 695.
(46) Benov, L.; Batinić-Haberle, I.; Spasojević, I.; Fridovich, I. *Arch. Biochem. Biophys.* **2002**, *402*, 159.
(47) Batinić-Haberle, I.; Spasojević, I.; Stevens, R. D.; Hambright, P.; Fridovich, I. *J. Chem Soc., Dalton Trans.* **2002**, 2689.
(48) Hambright, P.; Batinić-Haberle, I.; Spasojević, I. *J. Porphyrins Phthalocyanines*, submitted.

Table 1. HPLC Analysis Data of Mn(III) *meso*-Tetrakis(*N*-alkylpyridinium-2-yl)porphyrins and Corresponding Metal-Free Porphyrin Ligands and Zn(II) *meso*-Tetrakis(*N*-methyl(ethyl,*n*-hexyl)pyridinium-2-yl)porphyrins[a]

cmpd	solvent gradient %CH_3CN/min	fraction 1			fraction 2			fraction3			fraction 4			abundance ratio
		t_R	isomer	%	t_R	isomer	%	t_R	isomer	%	t_R	isomer	%	
H_2TM-2-PyP^{4+}	5−20/10	6.0	$\alpha\beta\alpha\beta$	21	6.5	$\alpha\alpha\beta\beta$	58	7.4	$\alpha\alpha\alpha\beta$	100	9.1	$\alpha\alpha\alpha\alpha$	20	1:2.9:5:1
Zn^{II}TM-2-PyP^{4+}	5−20/10	7.2	$\alpha\alpha\beta\beta$	50	7.6	$\alpha\beta\alpha\beta$	21	8.7	$\alpha\alpha\alpha\beta$	100	10.7	$\alpha\alpha\alpha\alpha$	40	2.4:1:4.8:1.9
Mn^{III}TM-2-PyP^{5+}	0−2/10	4.2	$\alpha\beta\alpha\beta$	22	6.3	$\alpha\alpha\beta\beta$	61[b]	6.6	$\alpha\alpha\alpha\beta$	100[b]	10.1	$\alpha\alpha\alpha\alpha$	14	1.6:4.4:7.1:1
H_2TE-2-PyP^{4+}	5−20/10	9.2	$\alpha\beta\alpha\beta$	12	9.3	$\alpha\alpha\beta\beta$	56	9.5	$\alpha\alpha\alpha\beta$	100	10.3	$\alpha\alpha\alpha\alpha$	39	1:4.7:8.3:3.3
Zn^{II}TE-2-PyP^{4+}	2−20/10	10.3	$\alpha\alpha\beta\beta$	57[b]	10.4	$\alpha\beta\alpha\beta$	9[b]	10.6	$\alpha\alpha\alpha\beta$	100	11.4	$\alpha\alpha\alpha\alpha$	40	6.3:1:11.1:4.4
Mn^{III}TE-2-PyP^{5+}	2−5/10	6.2	$\alpha\beta\alpha\beta$	12	7.0	$\alpha\alpha\beta\beta$	54	7.6	$\alpha\alpha\alpha\beta$	100	8.5	$\alpha\alpha\alpha\alpha$	30	1:4.5:8.3:2.5
H_2TBu-2-PyP^{4+}	10−30/10	8.9	$\alpha\alpha\beta\beta$	62	9.1	$\alpha\beta\alpha\beta$	13	9.2	$\alpha\alpha\alpha\beta$	100	9.9	$\alpha\alpha\alpha\alpha$	32	4.8:1:7.7:2.5
Mn^{III}TBu-2-PyP^{5+}	10−30/12	7.0	$\alpha\beta\alpha\beta$	13	7.3	$\alpha\alpha\beta\beta$	59	9.0	$\alpha\alpha\alpha\beta$	100	11.4	$\alpha\alpha\alpha\alpha$	27	1:4.5:7.7:2.1
H_2THex-2-PyP^{4+}	5−45/15	12.9	$\alpha\beta\alpha\beta$	18	13.0	$\alpha\alpha\beta\beta$	55	13.7	$\alpha\alpha\alpha\beta$	100	14.8	$\alpha\alpha\alpha\alpha$	28	1:3.1:5.6:1.6
Zn^{II}THex-2-PyP^{4+}	5−45/17	14.1	$\alpha\beta\alpha\beta$	15[b]	14.2	$\alpha\alpha\beta\beta$	56[b]	15.2	$\alpha\alpha\alpha\beta$	100	16.7	$\alpha\alpha\alpha\alpha$	35	1:3.6:6.5:2.3
Mn^{III}THex-2-PyP^{5+}	5−45/15	11.8	$\alpha\beta\alpha\beta$	10	12.0	$\alpha\alpha\beta\beta$	51	13.6	$\alpha\alpha\alpha\beta$	100	15.4	$\alpha\alpha\alpha\alpha$	30	1:5.1:10:3

[a] Where alkyl is methyl, ethyl, *n*-butyl, and *n*-hexyl. Fractions are enumerated according to their elution order (fraction 1, shortest retention time). t_R is the retention time in minutes; % corresponds to the percent relative abundance. Assignment of isomers was based on the HPLC elution pattern (retention times and peak intensities) and according to the assignment of isomers of H_2TM-2-PyP^{4+} verified by ^{1}H NMR and X-ray data. Conditions: YMC-Pack, ODS-AM reverse-phase column (3 μm particle size, 120 Å pore size, 150 mm long × 4.6 mm I. D.); column temperature, 45 °C; mobile phase A, 20 mM triethylamine, pH = 2.7 (adjusted with concentrated trifluoroacetic acid); mobile phase B, CH_3CN. [b] Incomplete separation.

Table 2. Structure Determination Summary

$C_{44}H_{38}N_8Cl_4O_{16}$	fw = 1074.64
a = 14.2846(15) Å	space group = $P2_1/c$ (monoclinic)
b = 22.2158(24) Å	T = −100 °C
c = 29.3690(30) Å	λ = 0.71073 Å
β = 95.374(2)°	(D_{calcd}) = 1.541 g cm^{-1}
V = 9279.1(17) Å^3	μ = 0.34 mm^{-1}
Z = 8	R_f = 0.077[a]
	R_w = 0.092

[a] $R_f = \sum|F_o - F_c|/\sum|F_o|$. $R_w = \sqrt{\sum[(wF_o - F_c)^2/\sum wF_o^2]}$.

Supporting Information. Detailed crystallographic data (crystal parameters, data collection and least-squares refinement, atomic coordinates, thermal parameters, bond lengths, and dihedral angles) are given in CIF file included in the Supporting Information.

Electrochemistry. Measurements were performed on a CH Instruments Model 600 voltammetric analyzer.[17,18] A small volume cell (Bioanalytical Systems, CC-5, 0.13 mm spacer) with a 6-mm-diameter glassy carbon button working electrode, Ag/AgCl reference electrode, and stainless steel auxiliary electrode was used. The potentials were standardized against the potassium ferrocyanide/ferricyanide.[18] The HPLC fractions were adjusted to 9.3 × 10^{-6} M in Mn^{III}TE-2-PyP^{5+} by addition of the mobile phase (4% acetonitrile, 20 mM triethylamine, pH 2.7 adjusted with concentrated trifluoroacetic acid) prior to neutralization by a concentrated buffer solution to a final concentration of 0.05 M sodium phosphate, 0.1 M NaCl, pH 7.4. The molar absorptivity was assumed to be equal for all four atropoisomers on the basis of the identical UV−vis spectra. Support for this assumption comes also from a direct correlation between redox potentials (independent of concentration) and catalytic rate constants for superoxide disproportionation (concentration dependent) shown later. A 0.2 mL aliquot of the described solution was purged with humidified argon for 15 min and transferred to the electrochemical cell with a gastight syringe (Hamilton Inc.). The scan rate was 0.1 V/s.

Catalysis of $O_2^{\bullet-}$ Dismutation. The cytochrome *c* assay is a convenient way to assess the ability of a given compound to catalytically scavenge $O_2^{\bullet-}$.[49] We have previously shown that the cytochrome *c* assay gives the same catalytic rate constant as does pulse radiolysis in the case of Mn^{III}TE-2-PyP^{5+} and several other compounds.[50]

The xanthine−xanthine oxidase reaction in the presence of oxygen produces $O_2^{\bullet-}$. Because of (self-)disproportionation (k = 1.5 × 10^5 M^{-1} s^{-1} at pH 7.4, 21 °C),[51,52] the "free" $O_2^{\bullet-}$ reaches a steady-state concentration. When cytochrome *c* is present in excess, it is reduced by $O_2^{\bullet-}$, the concentration of which drops to a new steady-state value. A linear increase in the concentration of reduced cytochrome *c* can be monitored at 550 nm. Addition of a compound able to react with $O_2^{\bullet-}$ at a rate appreciably higher than the self-disproportionation will decrease the rate of cytochrome *c* reduction. The difference between the observed rates of cytochrome *c* reduction in the presence and in the absence of the compound can be used to calculate the catalytic rate of "SOD-like" disproportionation ("dismutation") of $O_2^{\bullet-}$ for a given compound.

The four HPLC fractions, pooled from several consecutive injections of Mn^{III}TE-2-PyP^{5+}, were assayed in 0.05 M phosphate buffer, pH 7.8, 0.1 mM EDTA, ±15 μg/mL of catalase. The final concentration of each atropoisomer in the assay (10 μL in 3 mL total volume) was 5.0 × 10^{-8} M. The final concentrations of other components were the following: 40 μM xanthine, 2 nM xanthine oxidase, and 10 μM cytochrome *c*. Under such conditions, $O_2^{\bullet-}$ is produced at a rate of 1.2 μM min^{-1}. The reaction was initiated by the addition of xanthine oxidase. Absorbance at 550 nm was followed on a Shimadzu UV-2501PC spectrophotometer. Rate constants for the reaction of atropoisomers of Mn^{III}TE-2-PyP^{5+} with $O_2^{\bullet-}$ were calculated from $\Delta A/\Delta t$ slopes of the traces using the rate constant for cytochrome *c* reduction by $O_2^{\bullet-}$, k_{cytc} = 2.6 × 10^5 M^{-1} s^{-1}, as described in detail elsewhere.[50] Possible interference of test compounds with the xanthine−xanthine oxidase reaction (which produces $O_2^{\bullet-}$, H_2O_2, and urate) was examined by following the rate of urate accumulation at 295 nm in the absence of cytochrome *c*. All the measurements were done at 25 ± 1 °C. The catalytic rate constants are given in Table 3.

Tissue Binding. Fresh murine brain and liver tissue was homogenized in buffered saline containing 0.2 mM Mn^{III}TE-2-PyP^{5+}. The homogenate was delipidated by 3 extractions with chloroform/4% isoamyl alcohol, and the aqueous phase was filtered on a Millipore 3 kD cutoff centrifugal filter device (Microcon YM-3) for 1 h at 0 °C. The amount of each atropoisomer of Mn^{III}TE-2-PyP^{5+} in the ultrafiltrate was measured by HPLC as described earlier.

(49) McCord, J. M.; Fridovich, I. *J. Biol. Chem*. **1969**, *244*, 6049.
(50) Batinić-Haberle, I.; Spasojević, I.; Stevens, R. D.; Hambright, P.; Thorpe, A. N.; Grodkowski, N.; Neta, P.; Fridovich, I. *Inorg. Chem.* **2001**, *40*, 726.
(51) Riley, D. P.; Rivers, W. J.; Weiss, R. H. *Anal. Biochem*. **1991**, *196*, 344.
(52) Butler, J.; Koppenol, W. H.; Margoliash, E. *J. Biol. Chem*. **1982**, *257*, 10747.

Table 3. Half-Wave Redox Potentials ($E_{1/2}$ vs NHE, ± 3 mV Cyclic Voltammetry) and Second-Order Rate Constants for the Catalysis of Superoxide Disproportionation (k_{cat}, ± 5% Cytochrome *c* Competition Assay) of the Individual Atropoisomers of Mn^{III}TE-2-PyP^{5+} [a]

fraction of Mn^{III}TE-2-PyP^{5+}	k_{cat}, $10^7\,M^{-1}s^{-1}$	$E_{1/2}$, mV (vs NHE)
1 ($\alpha\beta\alpha\beta$)	5.53	220
2 ($\alpha\alpha\beta\beta$)	6.34	234
3 ($\alpha\alpha\alpha\beta$)	6.19	232
4 ($\alpha\alpha\alpha\alpha$)	6.84	240
mixture before separation	5.78	228

[a] Conditions given in Experimental Section.

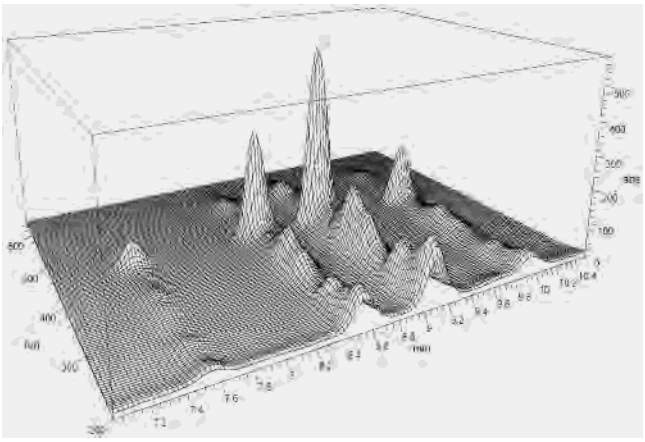

Figure 1. Multiwavelength UV−vis chromatogram obtained after reverse-phase HPLC separation of rotational (atropo-) isomers of Mn^{III}TE-2-PyP^{5+}. Conditions as in Table 1.

Results

Mn^{III}TE-2-PyP^{5+}. HPLC Separation. Figure 1 shows time-resolved UV−vis spectra obtained during the elution of Mn^{III}TE-2-PyP^{5+}. Four distinctive fractions can be observed with identical UV−vis spectra as expected for rotational (atropo-) isomers. Collected fractions are inert to isomerization ("scrambling") for at least one month at room temperature, and it took 16 days at 90 °C for 50% of statistically least preferable fractions $\alpha\beta\alpha\beta$ and $\alpha\alpha\alpha\alpha$ to be converted to the other isomers. Data are given in the Supporting Information, Figures S3 and S4.

Mn^{III}TE-2-PyP^{5+} is paramagnetic and thus not suitable for ^{1}H NMR measurements. Because very similar behavior in HPLC and in thermal stability was observed for methyl analogues of the metal-free ligand, H_2TM-2-PyP^{4+}, and for ZnTM-2-PyP^{4+}, quantitative HPLC separation and ^{1}H NMR analysis of their atropoisomers were performed to help the identification of HPLC fractions of manganese complexes and of higher metal-free alkyl analogues. The *N*-methyl compounds were chosen because of the relative simplicity of their ^{1}H NMR spectra. On the basis of the identity of the H_2TM-2-PyP^{4+} fractions (Figure 2A,B) and a similarity in the intensity pattern (closely resembling a statistically expected distribution of isomers), the fractions of Mn^{III}TE-2-PyP^{5+} were assigned in order of their elution as follows: fraction 1, $\alpha\beta\alpha\beta$; fraction 2, $\alpha\alpha\beta\beta$; fraction 3, $\alpha\alpha\alpha\beta$; and fraction 4, $\alpha\alpha\alpha\alpha$ (Scheme 1, Table 1). Separated fractions were kept at 90 °C for weeks; fraction 3 was the most resistant to isomerization while the other fractions showed a tendency to isomerize into fraction 3. This observation is in accordance with the expected highest probability of formation of the $\alpha\alpha\alpha\beta$ isomer (data given in the Supporting Information, Figure S4).

Electrochemistry. Cyclic voltammetry of atropoisomers of Mn^{III}TE-2-PyP^{5+} resulted in reversible voltammograms corresponding to the Mn^{III}/Mn^{II} redox couple. A measurable difference in metal-centered half-wave potentials, $E_{1/2}$, was found among atropoisomers (Table 3).

Catalysis of $O_2^{\bullet-}$ Disproportionation. Reactivity of Mn^{III}-TE-2-PyP^{5+} atropoisomers toward $O_2^{\bullet-}$ was probed by the cytochrome *c* assay. Repeated experiments showed a very small, yet measurable, difference among the atropoisomers (Table 3). No interference with the xanthine−xanthine oxidase reaction was observed.

Tissue Binding Properties. A brief study of tissue binding of Mn^{III}TE-2-PyP^{5+} atropoisomers by murine brain and liver was undertaken to address the distribution of the atropoisomers in vivo. In terms of the relative amount of atropoisomers, the HPLC chromatogram of the filtrate was identical to one of the original buffered saline solutions of Mn^{III}TE-2-PyP^{5+}prior to tissue homogenization (data not shown). Hence, there was no preferential binding of any one atropoisomer.

H_2TM-2-PyP^{4+}. HPLC Separation. Figure 2A shows a chromatogram of a H_2TM-2-PyP^{4+} sample mixture (top trace) and reinjected fractions of atropoisomers. The fractions are practically inert to isomerization ("scrambling") at room temperature or for hours at reflux temperature of 90 °C (data not shown). It is noteworthy, however, that, when the collected fractions were freeze-dried and then dissolved in H_2O or D_2O, almost complete isomerization occurred. Isomerization occurred to much lesser extent upon freeze-drying of fractions containing a nonvolatile anion (0.1 M NaCl or 0.1 M NaH_2PO_4) or upon fast evaporation at 60 °C under vacuum followed by drying overnight under vacuum at room temperature. Furthermore, no isomerization was observable for frozen fractions kept overnight at −80 °C at atmospheric pressure (data given in the Supporting Information, Figure S5). Thus, for the ^{1}H NMR experiment, the mobile phase was removed at room temperature under mild vacuum almost to dryness and then replaced by D_2O. Chromatograms of the solutions so prepared are shown in Figure 2A.

^{1}H NMR Identification. The close proximity of a positive charge to *N*-methyl hydrogens (refer to Scheme 1) produces a measurable ^{1}H NMR chemical shift. It has been shown previously[15] and confirmed in this work that the chemical shift comes mainly from the orientation of *adjacent* (neighboring) *cis* (on the same side of the porphyrin ring plane) charges and that the effect of more remote charges can be neglected for identification purposes. Consequently, there are three possible positions of *N*-methyl hydrogen bands in the ^{1}H NMR spectrum regarding the number of *cis* neighboring charges: no neighbors (weak chemical shift, low ppm values), one neighbor (moderate chemical shift), and two neighbors (strong chemical shift, high ppm values). Thus, theoretically, ^{1}H NMR spectra for the *N*-methyl protons in

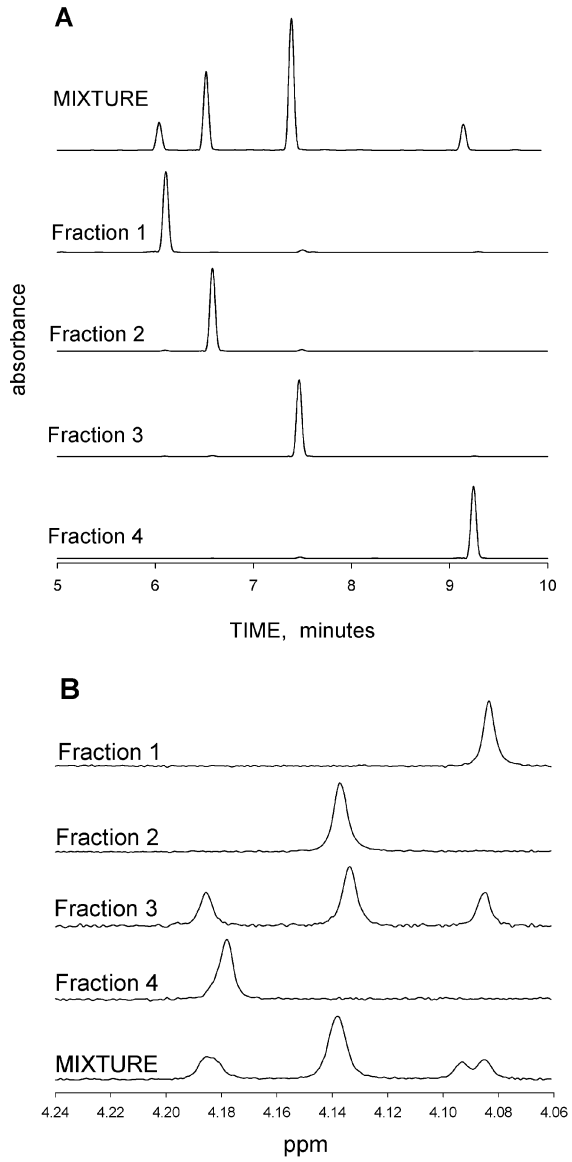

Figure 2. A: HPLC/UV−vis (414 nm) analysis of H_2TM-2-PyP^{4+} original solution (mixture) and of reinjected individual fractions (1−4, in order of elution) prior to ^{1}H NMR measurements. Conditions as in Table 1. B: ^{1}H NMR spectra of individual fractions (1−4) of H_2TM-2-PyP^{4+} and a spectrum of the original solution (mixture) before HPLC separation and after replacement of solvent by D_2O.

a given isomer should be as follows: αααα, 1 resonance, strongly shifted downfield (each α with two neighboring charges); ααα*β*, 3 resonances, one strongly shifted downfield (middle α), one moderately shifted of twice the intensity (two side αs), and one weakly shifted (one *β*, no neighboring *cis* charges); αα*ββ*, 1 resonance, moderately shifted (four identical groups of protons each with one neighboring *cis* charge); and α*β*α*β*, 1 band, weakly shifted (four identical groups of protons each without neighboring *cis* charges). Figure 2B presents ^{1}H NMR spectra of HPLC fractions 1−4 and of the original mixture prior to HPLC separation of H_2-TM-2-PyP^{4+}. The identification of the fractions based on the described reasoning is straightforward: fraction 1 is α*β*α*β*, fraction 2 is αα*ββ*, fraction 3 is ααα*β*, and fraction 4 is αααα (longest retention time). It was possible to reconstruct the spectrum of the mixture in terms of intensities from

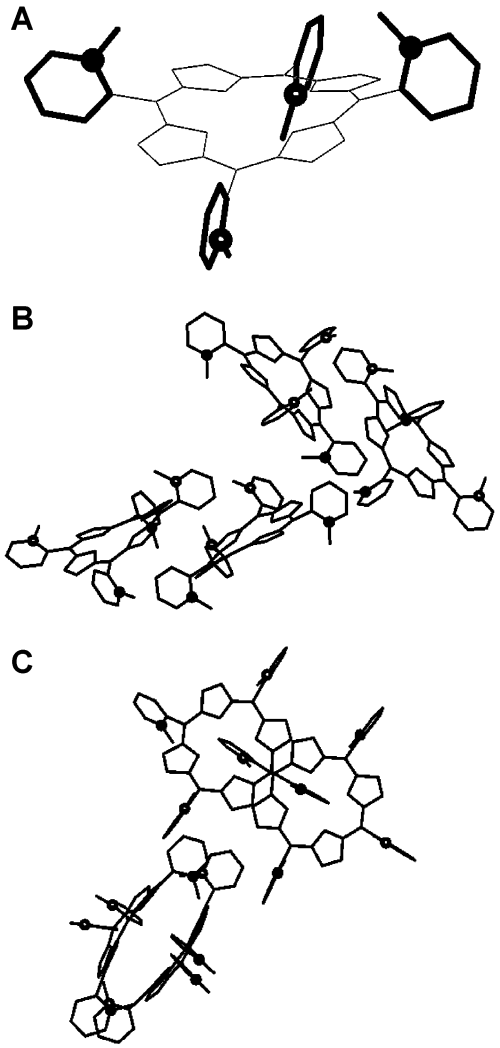

Figure 3. A: X-ray crystal structure of α*β*α*β*-H_2TM-2-PyP^{4+} depicted as a simplified drawing of one of the two crystallographic structures found in the crystallographic cell; pyridyl nitrogens drawn as balls, dotted atoms are at the same side of the porphyrin plane. ORTEP diagrams and other relevant information given in the Supporting Information. B: A simplified drawing to emphasize the crystal packing; only four, out of total eight molecules found in the crystallographic cell, are shown. C: A different view of the same cluster as in B.

spectra of individual fractions and abundance of each fraction in the original mixture. The spectrum of the mixture also reveals a considerable "coupling" between the neighboring and the opposite *cis* (α) and/or *trans* (*β*) charges which gives rise to 5 recognizable resonances in the ^{1}H NMR spectrum of the original mixture, instead of the 3 predicted, on the basis of the assumption that only a neighboring charge is responsible for the chemical shift.

X-ray Structure of α*β*α*β* Isomer. The X-ray crystal structure of H_2TM-2-PyP^{4+} confirmed our ^{1}H NMR identification of fraction 1 as the α*β*α*β* isomer (Figure 3A). There are 8 molecules per crystallographic cell with 2 crystallographically different porphyrin molecules which primarily differ in orientation of the pyridyl rings relative to the "mean plane" of the porphyrin ring (66.7−84.9°; Table S3, Supporting Information). The two porphyrin molecules apparently form a "dimer" which then packs into the crystal lattice (Figure 3B,C). The inner nitrogen atoms of the porphyrin

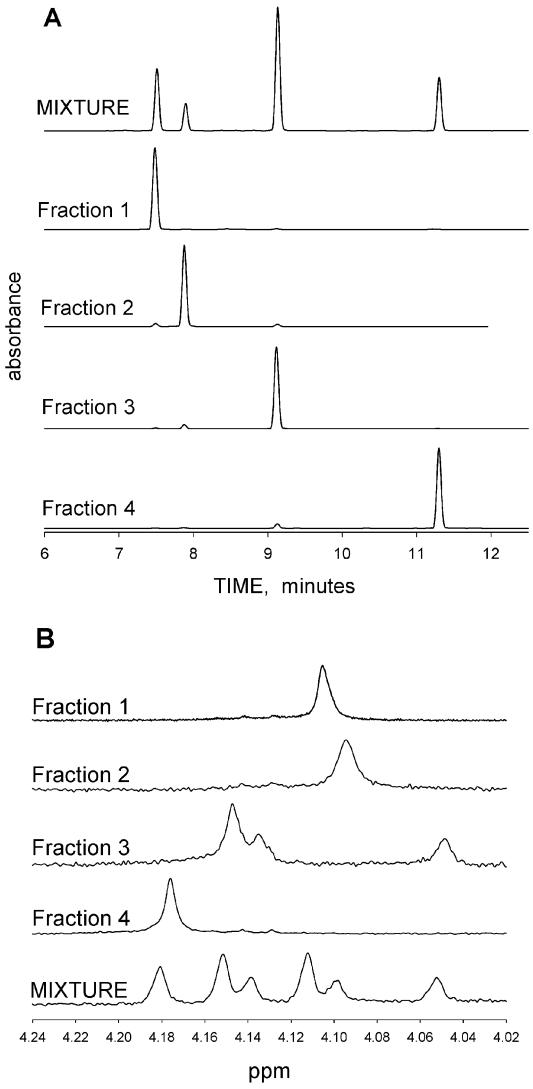

Figure 4. **A**: HPLC/UV−vis (426 nm) analysis of ZnTM-2-PyP^{4+}; original solution (mixture) and of reinjected individual fractions (1−4, in order of elution) prior to ^{1}H NMR measurements. Conditions as in Table 1. B: ^{1}H NMR spectra of individual fractions (1−4) of ZnTM-2-PyP^{4+} and spectrum of the original solution (mixture) before HPLC separation and after replacement of solvent by D_2O.

ring fit almost perfectly into a "mean plane". However, the porphyrin ring is greatly distorted into a saddlelike shape as a consequence of the *meso*-bridges (bearing pyridyl groups) opposite to each other being above or below the plane (Figures S1 and S2; Tables S1 and S2 in the Supporting Information). Hydrogen atoms bound to the inner nitrogen atoms of the porphyrin plane were located from the difference electron density map.

Zn Porphyrins. Figure 4 shows the ^{1}H NMR spectra of HPLC fractions 1−4 and of a mixture of atropoisomers of ZnTM-2-PyP^{4+}. The picture is quite different than in the case of the metal-free ligand. The first HPLC fraction is of higher abundance than the second one, which is an unusual feature seen also in the case of ZnTE-2-PyP^{4+} and the metal-free butyl analogue ligand, H_2TBu-2-PyP^{4+}. However, although the separation of fractions 1 and 2 was incomplete in the case of the hexyl analogue of the Zn compound, ZnTHex-2-PyP^{5+}, the shoulder of the lower abundance on the shorter retention time side of the (first + second) fraction peak suggests that the retention exchange did not happen.

The question is whether the first fraction of ZnTM-2-PyP^{4+} is still $\alpha\beta\alpha\beta$ but with an increased abundance (upon metalation with Zn) or whether the $\alpha\beta\alpha\beta$ and $\alpha\alpha\beta\beta$ isomers have just exchanged their retention properties. An unequivocal assignment was complicated by the ^{1}H NMR spectrum of the third fraction ($\alpha\alpha\alpha\beta$) in which the resonance of low intensity at 4.147 ppm (presumably originating from middle α) lies at a lower ppm value than the higher intensity band at 4.152 ppm.

There are strong arguments that the retention exchange is the likely scenario. First, fractions $\alpha\beta\alpha\beta$ and $\alpha\alpha\beta\beta$ are very similar, both having two *N*-methyl groups above and two *N*-methyl groups below the porphyrin plane, and are thus expected to be the most difficult to separate. The chromatograms of H_2TM-2-PyP^{4+} (Figure 2A) and of all other homologous compounds of longer *N*-alkyl chains (Table 1) support this statement. It seems likely that, having very narrow retention times, the two isomers upon metalation by Zn(II) may "flip" their retention on the column. Second, the ^{1}H NMR spectra of the first and second fractions follow the expected order in ppm values (as well as the low-ppm resonance (β) in fraction 3). If fraction 1 is assigned to $\alpha\alpha\beta\beta$ (instead of $\alpha\beta\alpha\beta$), it should have a resonance at higher ppm than fraction 2 (now $\alpha\beta\alpha\beta$). Figure 2B shows that it does. Third, enrichment in one isomer is not likely to occur upon metalation. It does not occur upon metalation by Mn(III) of all the ligands studied and, in the case of the *N*-ethyl analogue, not even when the metalation was done in the presence of silica (data not shown). Finally, there is an obvious pattern observed where shorter alkyl chains cause retention time exchange between fractions 1 and 2 but the longer alkyl chains do not. Thus, both ^{1}H NMR and HPLC data (Figure 4) suggest that Zn compounds might have some peculiar structural features when compared to their Mn and metal-free analogues.

Other *N*-alkylpyridyl Analogues. By changing only the amount of acetonitrile in the mobile phase, we were able to completely separate all four atropoisomers of H_2TM-2-PyP^{4+}, ZnTM-2-PyP^{4+}, ZnTE-2-PyP^{4+}, H_2TE-2-PyP^{4+}, Mn^{III}TE-2-PyP^{5+}, H_2TBu-2-PyP^{4+}, Mn^{III}TBu-2-PyP^{5+}, H_2THex-2-PyP^{4+}, and Mn^{III}THex-2-PyP^{5+}. The only exceptions are Mn^{III}TM-2-PyP^{5+} and ZnTHex-2-PyP^{4+}. In the case of the former, an almost complete separation (~95%) of $\alpha\alpha\beta\beta$ and $\alpha\alpha\alpha\beta$ isomers was achieved (Table 1). The $\alpha\beta\alpha\beta$ and $\alpha\alpha\beta\beta$ atropoisomers of ZnTnHex-2-PyP^{4+} were practically inseparable.

Discussion

Because Mn^{III}TE-2-PyP^{5+} is a potential therapeutic agent, it was desirable to develop an HPLC method for its detection in biological fluids and tissues. Rotational (atropo-) isomers impose a problem regarding their potentially different chemical and physical properties. There are several questions that this work was designed to answer: Is it possible to separate and isolate individual isomers of Mn^{III}TE-2-PyP^{5+} (and other Mn(III), Zn(II), and metal-free ligand analogues)?

What is the identity of the fractions, and what is the order of elution on the reverse-phase column? How stable are individual isomers toward isomerization ("scrambling")? How stable are the isomers toward the stationary phase in the HPLC column; that is, is the distribution or existence of fractions influenced by the interaction with the stationary phase? What is the reactivity of each fraction toward $O_2^{\bullet-}$? Are their redox potentials the same? How stable is the mixture toward further change in the distribution of atropoisomers, especially in vivo?

Four factors made the separation of the atropoisomers of Mn^{III}TE-2-PyP^{5+} possible: (1) recent advances in reverse-phase HPLC column technology, including the high degree of silanization which minimizes the interaction of highly (positively) charged solutes with free hydroxyl groups of the column packing; (2) the presence of an ion-pairing agent (20 mM trifluoroacetic acid) which further minimizes such interactions; (3) increased temperature (45 °C) which reduces the viscosity of the mobile phase, thus increasing the diffusion coefficient of the solute and thus increasing the efficiency (rate) of the separation for a given length of the column; (4) sufficient inertness of the atropoisomers toward isomerization ("scrambling") at the operating temperature.

The isolated atropoisomers in aqueous solution are practically inert to isomerization for at least one month at room temperature. (The inertness toward isomerization of the Ni(II), Cu(II), and Zn(II) atropoisomers of the same porphyrin for greater than one month was previously also observed by Kaufmann et al.)[15] When reinjected back into the HPLC system, the fractions reproduced their retention times, and no other fractions appeared in the chromatogram. This result is important in terms of a concern that the interaction with the stationary phase may influence the distribution of atropoisomers; that is, the measured ratio may not realistically reflect the distribution in the original solution. The identity of HPLC fractions of Mn^{III}TE-2-$PyP^{5+}$was indirectly determined from ^{1}H NMR spectra and the X-ray structure ($\alpha\beta\alpha\beta$ isomer) of H_2TM-2-PyP^{4+}, and by utilizing the obvious analogy in the HPLC distribution pattern of both compounds (Table 1). An important conclusion is that the more grouped the *N*-alkyl groups are (e.g., $\alpha\alpha\alpha\alpha$ isomer), the longer the retention time on the reverse-phase column.

The simplicity of the ^{1}H NMR spectrum of the *N*-methyl group made identification of H_2TM-2-PyP^{4+} straightforward. Still, the opportunity to obtain a crystal structure of the $\alpha\beta\alpha\beta$ isomer provided verification of the interpretation of the ^{1}H NMR spectra. Thus, even when the elution pattern was partially reversed, as in the case of ZnTM-2-PyP^{4+} (Table 1), we could identify the fractions on the basis of HPLC/^{1}H NMR data alone. The HPLC column elution order (as well as ^{1}H NMR spectra) may be affected by the rotational lability of the pyridyl rings relative to the porphyrin ring (which can be inferred from somewhat "arbitrary" positions of pyridyl rings in the X-ray structure; Figure 4), distortion of the porphyrin ring (due to metalation and/or different symmetry of the isomers), and axial coordination of solvent or anions. One or more of these effects can account for the anomalous behavior observed in the case of ZnTM-2-PyP^{4+} (elution order and ^{1}H NMR data), and ZnTE-2-PyP^{4+} and H_2TBu-2-PyP^{4+} (elution order) (Table 1). Because the previously published X-ray structure of the Cu(II) complex with the same porphyrin ligand dealt with a different atropoisomer ($\alpha\alpha\alpha\beta$), the assessment of the impact of the metal on the porphyrin ring distortion was not possible.

Of particular interest was the question of whether individual rotational isomers of Mn^{III}TE-2-PyP^{5+} exhibited different reactivity toward $O_2^{\bullet-}$. The compound, as a mixture of isomers, exhibits a high superoxide-dismutase-like potency. It could be argued, however, that the $\alpha\alpha\alpha\alpha$ isomer might be more reactive than the other isomers because it most closely resembles the superoxide dismutase active center with its positively charged "cone" which is believed to facilitate its reaction with $O_2^{\bullet-}$.[53] This proved not to be the case. Only a very modest difference in reactivity toward superoxide was observed which can be explained by a small difference in metal-centered redox potentials found among the atropoisomers (Table 3). Thus, atropoisomers obey the structure−activity relationship between the catalytic rate constant for the $O_2^{\bullet-}$ dismutation and the metal-centered redox potential that we previously established for water-soluble porphyrins, including Mn^{III}TM(E)-2-PyP^{5+} as a mixture of atropoisomers.[18] For each 120 mV increase in $E_{1/2}$ for the Mn(III)/Mn(II) redox couple, there is a 10-fold increase in k_{cat}, consistent with the Marcus equation[54,55] for an outer-sphere electron transfer. The difference in redox potential likely originates either from slightly different lipophilicity (solvation effects)[47] or from a difference in porphyrin ring distortion.

The inertness toward isomerization and very similar reactivity and tissue binding properties of atropoisomers justify testing the compound either as a single isomer or as a mixture of isomers as a possible therapeutic agent.

Acknowledgment. The authors are grateful for financial support from NIH 1R01DK59868-01, the ALS Association, and Aeolus/Incara Pharmaceuticals, Research Triangle Park, NC. I.S. is grateful for support from the Christopher Reeve Paralysis Foundation, BAR1-0103-1. Helpful discussions with Ines Batinić-Haberle, and assistance with ^{1}H NMR experiments by Anthony A. Ribeiro, Duke University Medical Center, are much appreciated.

Supporting Information Available: Additional figures and tables. Crystallographic data in CIF format. This material is available free of charge via the Internet at http://pubs.acs.org.

IC025556X

(53) Getzoff, E. D.; Cabelli, D. E.; Fisher, C. L.; Parge, H. E.; Viezzoli, M. S.; Banci, L.; Hallewell, R. A. *Nature* **1992**, *358*, 347.
(54) Bennett, L. E. *Prog. Inorg. Chem.* **1973**, *18*, 1.
(55) Marcus, R. A. *Annu. Rev. Phys. Chem*. **1964**, *15*, 155.